Red-shifted iLOV mutants have decreased brightness disrupting their use in live cell imaging

Pierre Wehler[1,2] and Mehmet Ali Öztürk[1,2,*]

1 Institute of Biology II, University of Freiburg, Schänzlestraße 1, 79104 Freiburg, Germany

2 Centers for Biological Signalling Studies BIOSS and CIBSS, University of Freiburg, Schänzlestraße 1, 79104 Freiburg, Germany

*** Corresponding author:** Mehmet Ali Öztürk, Institute of Biology II University of Freiburg, Schänzlestraße 1, 79104 Freiburg, +49 761 203 2787, mehmet.oeztuerk@bioss.uni-freiburg.de

Abstract

iLOV is a flavin mononucleotide (FMN)-binding fluorescent protein (FbFP) with excitation and emission spectra similar to those of the green fluorescent protein (GFP). Importantly, contrary to GFP, iLOV fluoresces independently of molecular oxygen, making its usage in low-oxygen conditions possible. Moreover, iLOV is smaller than GFP, increasing the likelihood of retaining full functionality when creating fusions with proteins of interest. Nonetheless, GFP remains to date the most widely used FP in molecular biology, also due to the availability of multiple spectrally tuned variants allowing multi-color imaging experiments. To expand the range of applications of iLOV, spectrally tuned red-shift variants are desirable to have reduced phototoxicity and better tissue penetration. Here we experimentally tested two iLOV mutants, $iLOV^{L470T/Q489K}$ and $iLOV^{V392K/F410V/A426S}$, which were previously computationally proposed to have red-shifted excitation and emission spectra. We found that only the triple mutant has moderately red-shifted excitation and emission spectra. Both mutants exhibit strongly decreased brightness, which impedes their employment in live cell imaging. Finally, we show that the single V392K mutation suffices to red-shift the emission spectrum as well as abolishes fluorescence of iLOV.

Introduction

Fluorescent proteins (FPs) have revolutionized cell biology by enabling researchers to investigate dynamic cellular processes in real time[1]. The most widely used FP is GFP and its spectrally shifted and/or engineered variants[1], for instance further optimized to more rapidly mature (sfGFP)[2] or more brightly fluoresce (mNeonGreen)[3]. Despite their usefulness, FPs of the GFP family have some limitations: (a) they depend on molecular oxygen for chromophore formation, which impedes their

use to visualize processes under hypoxic or anoxic conditions[4–6]; (b) are relatively large (~25 kDa), which can be problematic in some applications[7], (c) and are mostly sensitive to pH[8]. While pH-resistant GFP variants have been engineered[8], oxygen-dependence and size are unchangeable features. FMN-binding fluorescent proteins (FbFPs) overcome these limitations and thus are valuable alternatives to GFP and its variants[9,10]. FbFPs consist of a small light oxygen voltage (LOV) domain (~11 kDa) modified to emit green fluorescence when light in the UV-A-blue range reaches the non-covalently bound FMN chromophore[11].

One prominent FbFP is iLOV, a derivative of the LOV2 domain of *Arabidopsis thaliana*[7]. Several rounds of DNA shuffling led to a mutation in a key cysteine residue and triggering the emission of fluorescence[7]. So far, all experimentally obtained FbFPs share spectral features similar to GFP [12]. However, FbFPs possessed relatively weak fluorescent intensity until very recently[13,14]. Engineering a red-shifted FbFP could address this problem by shifting the excitation and emission peaks away from the cellular autofluorescence. Additionally, potential phototoxicity due to prolonged blue-light application could be minimized, and applications which require tissue penetration could be enabled. Moreover, a red-shifted FbFP variant could be used orthogonally to other FbFPs and would potentially allow for multicolor imaging and FRET-based biosensors.

By using the observation of the presence of positively charged residues in close proximity of the chromophore, which is a motif in red-light fluorescent proteins like Rtms5[15] and mKeima[16], Khrenova et al. previously applied quantum mechanics / molecular mechanics (QM/MM) simulations and proposed that iLOV^{Q489K} mutant could represent ~50 nm red shift of excitation and emission band maxima of iLOV[17]. While their rationale was based on the design of positively charged amino group of K489 next to chromophore stabilizing the π- electron system of the FMN in the excited state, later Davari et al. computationally and experimentally showed that K489 is mostly populated in an open conformer which is far from the chromophore and in fact iLOV^{Q489K} is blue shifted[18]. In a follow up study, Khrenova et al. applied a second round of QM/MM calculations to find iLOV mutants that have more stabilized lysine residues next to the chromophore than previous iLOV^{Q489K} mutant and they proposed that iLOV$^{L470T/Q489K}$ and iLOV$^{V392K/F410V/A426S}$ mutants could result in ~50 nm red shift for both excitation - emission spectrum of iLOV[19]. A shift by this size would open up new potential applications for iLOV and FbFPs in general. Here, we wanted to experimentally validate these findings and characterize the spectral properties of the two predicted mutants.

Material and Methods

Plasmid construction

Constructs were generated using classical restriction enzyme cloning or golden gate cloning. Constructs and oligonucleotide sequences used in this study are listed in Supplementary Tables I and II, respectively.

The *ilov* gene was amplified with primers OL01 and OL02 from iLOV-N1, gift from Michael Davidson (Addgene plasmid #54673; http://n2t.net/addgene:54673; RRID:Addgene_54673) and cloned into pcDNA3.1(+) using HindIII and EcoRI restriction sites, yielding plasmid PL01. PL01 was used as a template to clone all iLOV variants used in this study. Single-point mutations Q489K and V392K were created via overhang PCR using primer pairs OL01-OL03 and OL02-OL04 yielding PL02 and PL04, respectively. The L470T mutation was introduced into PL02 using golden gate cloning. The first fragment was amplified with primers OL01 and OL10, the second fragment with primers OL09 and OL03. Amplicons were digested with HindIII and BpiI, or BpiI and EcoRI, respectively, and cloned into pcDNA3.1(+) yielding PL03. The A426S mutation was inserted into PL04 by addition of a XbaI restriction site into the coding sequence. The first part was amplified using primers OL04 and OL06, the second part was amplified using primers OL05 and OL02 and cloned into pcDNA3.1(+) yielding PL05. The F410V mutation was introduced using golden gate cloning. The first fragment was amplified with primers OL04 and OL08, the second fragment with primers OL02 and OL07. Amplicons were digested with HindIII and BpiI or BpiI and EcoRI, respectively, and cloned into pcDNA3.1(+) yielding PL06.

For expression in and purification from *Escherichia coli*, the *ilov*, $ilov^{L470T/Q489K}$, $ilov^{V392K}$ and $ilov^{V392K/F410V/A426S}$ genes were amplified using primers OL11 or OL12 (for mutants containing the V392K mutation) and OL13, and then cloned into pET28a using NdeI and XhoI restriction sites, yielding PL07-PL10. The sequence of all constructs was verified using Sanger sequencing.

Protein expression and purification

Each pET28a plasmid harbouring one iLOV construct was transformed into *E. coli* Rosetta™ (DE3) pLysS cells for protein expression. A large expression culture (1L LB containing 0.1 mg/mL kanamycin) was started with an optical density (OD_{600}) of 0.05 from an overnight culture and was grown at 37 °C at 180 rpm until it reached an OD_{600} of 0.8. IPTG (Isopropyl-β-D-thiogalactopyranosid) was then added to the culture to a final concentration of 1 mM, and the

culture was further grown at 18 °C overnight. The next morning, cells were harvested via centrifugation at 5000 × g for 30 minutes. The pellets were resuspended in lysis buffer (50 mM potassium phosphate pH 8.0, 300 mM NaCl and 10 mM imidazole pH 8.0) containing one tablet of cOmplete™ protease inhibitor cocktail (Roche), and lysed by sonication. The lysate was clarified by centrifugation at 20,000 rpm at 4 °C and loaded onto an IMAC nickel column (1 mL) using the Bio-Rad NGC automated liquid chromatography system. The column was washed with wash buffer (same as lysis buffer but with 20 mM imidazole and 10 % glycerol) and eluted with elution buffer (same as lysis buffer but the pH of potassium phosphate is 7.5 with further addition of 10 % glycerol and 500 mM imidazole). Finally, the elution buffer was replaced with a storage buffer (50 mM HEPES-KOH pH 7.25, 150 mM KCl, 10 % glycerol and 0.1 mM EDTA pH8.0) using a P-6 desalting column (10 mL). The purified protein was aliquoted and the aliquots were stored at −80 °C.

Spectroscopy

Excitation and emission spectra were measured with a fluorescence spectrophotometer (Tecan Infinite M200). 200 µL of each purified protein (final concentration = 333 µg/mL) were dispensed into a well of a black 96-well plate. 200 µL of the storage buffer was used as blank. For excitation spectra, excitation was carried out from 420 nm to 490 nm and fluorescence was measured at 530 nm (step size 1 nm). For emission spectra, excitation was fixed at 450 nm, and the fluorescent signal was measured from 480 nm to 570 nm (step size 2 nm).

Cell culture and transient transfection

Human non-small cell lung carcinoma cells (H1299; kindly provided by Alexander Loewer, Max Delbrück Center for Molecular Medicine, Berlin) were maintained in RPMI 1640 media supplemented with 10% foetal bovine serum, 100 U/ml penicillin and 100 µg/ml streptomycin. Cells were cultivated at 37 °C and 5% CO_2 and were passaged when reaching ∼90% confluence.

For microscopy experiments, H1299 cells were seeded in µ-Slide 8-well chambers (Ibidi GmbH) at densities of ~15000 per well. The following day, the samples were transfected with 150 ng of construct DNA using Lipofectamin 2000 (ThermoFisher Scientific) according to the manufacturer's manual. Samples were imaged 36 hours post-transfection.

Fluorescence microscopy

Cells were imaged at 37 °C and 5% CO_2 in µ-Slide 8 well chambered coverslips (Ibidi GmbH) on a Zeiss AxioObserver wide-field microscope equipped with an incubation chamber, a 40x air objective (0.7 NA), the Colibri.2 LED light source and a filter set for eGFP.

Data processing

Analysis of spectral data was carried out using Python[20], particularly the pandas library[21]. The blank was subtracted from the respective values. If not mentioned otherwise, the respective spectra were then normalized to their highest value. Plots were generated using the matplotlib library[22].

Results

in vitro characterization of iLOV$^{L470T/Q489K}$ and iLOV$^{V392K/F410V/A426S}$

In order to verify the computationally predicted shift in the excitation and emission spectra of the two proposed iLOV mutants (Figure 1), we cloned iLOV$^{L470T/Q489K}$ and iLOV$^{V392K/F410V/A426S}$ into a bacterial expression plasmid carrying an N-terminal 6xHis-tag and purified the iLOV variants via nickel affinity chromatography. In contrast to the computations of Khrenova et al.[19], our experiments indicated that the excitation peak of iLOV$^{L470T/Q489K}$ was in fact slightly blue shifted (Figure 2). The emission peak was shifted only by 6 nm. The second mutant, iLOV$^{V392K/F410V/A426S}$, was red-shifted in both excitation and emission peaks. However, the shift of the excitation maxima was only minor. As a result, among computationally proposed mutants, only triple mutant has shown a slight excitation and emission red-shift.

Next to the comparably small shift in the spectra, we noticed a strong reduction in fluorescent intensity in the two iLOV mutants compared to iLOV (Figure 3). This is particularly problematic due to low brightness of iLOV itself and FbFPs in general[7,12]. The fluorescent intensity of iLOV$^{L470T/Q489K}$ was reduced around 10-fold, the intensity of iLOV iLOV$^{V392K/F410V/A426S}$ even around 100-fold compared to WT iLOV. Noteworthy, only the pellet of *E. coli* expressing WT iLOV was coloured greenish, yet none of the mutants exhibited any colour. This supports the decrease of fluorescent intensity.

The reduction in fluorescent intensity is likely caused by introduced mutations, either due to a direct effect on the protein's interaction with its chromophore or indirectly causing an impairment of

protein folding. To assess the purity of the purified iLOV variants, we visualized the proteins on a SDS-Gel (Supplementary Figure 1). While iLOV is exclusively monomeric, mutants apparently can also form oligomers. Yet the majority of the purified protein is still monomeric, therefore the reduction of fluorescent intensity cannot be accounted for by the low fraction of oligomerized proteins alone.

iLOV^{V392K} is similar in spectral properties but brighter than iLOV$^{V392K/F410V/426S}$

Of the two characterized mutants, mutant iLOV$^{V392K/F410V/A426S}$ exhibited more favourable red-shift spectral properties. However, its brightness was severely reduced compared to WT iLOV. To evaluate the contribution of an individual mutation to the spectral shift and the reduced brightness, we decided to characterize iLOV^{V392K} single mutant, which has neither computationally nor experimentally characterized before.

The excitation - emission spectral properties of iLOV^{V392K} and iLOV$^{V392K/F410V/A426S}$ were similar (Figure 4AB, Table I). Apparently, mutation of V392K was sufficient to cause the red-shift in excitation peak to the same extent as iLOV$^{V392K/F410V/A426S}$, and a mildly stronger shift in the emission maxima. Compared to the triple mutant, iLOV^{V392K} was about 10-fold brighter, having a comparable intensity to iLOV$^{L470T/Q489K}$ (Figure 4CD). While this increase is strong, the fluorescent intensity is still about 10-fold lower than the WT iLOV, which has a comparably low brightness itself [12]. To further evaluate whether the increase in brightness is sufficient for *in vivo* experiments, we decided to test the iLOV variants in mammalian cells.

In vivo characterization of iLOV variants

We selected the non-small lung cancer cell line H1299 for evaluating the *in vivo* fluorescent signal of iLOV mutants. In a first experiment, cells expressing iLOV variants (WT, V392K, L470T/Q489K and V392K/F410V/A426S) for 20 hours did not exhibit any fluorescence, even WT iLOV was not visible (data not shown). Given the weak brightness, we reasoned to increase the amount of transfected DNA (10 nm to 150 ng) and increase expression time from 20 to 36 hours. The adaption of the transfection protocol led to a visible fluorescent signal in cells expressing WT iLOV (Figure 5). Noteworthy, photobleaching occurred quickly in WT iLOV as previously reported [7,23]. However, none of the samples expressing one of three iLOV mutants exhibited any fluorescent signal.

Discussion

In this study, we set out to characterize the excitation and emission spectra of the two iLOV mutants iLOV$^{L470T/Q489K}$ and iLOV$^{V392K/F410V/A426S}$, which were computationally predicted to be red-shifted up to 50 nm[19]. However, our *in vitro* validation could not support the predicted extent of the shifts. Similarly, in a first study Khrenova et al. predicted the single mutant iLOV^{Q489K} to be shifted in excitation and emission peak by 52 nm and 97 nm, yet the measured excitation and emission peaks exhibited a blue-shift of about 10 nm [17,18], highlighting the disagreement between prediction and experimental validation. Even though the QM/MM modelling approach was subsequently updated according to the experimental validation of iLOV^{Q489K} [19], it seems to not capture the complexity of the interaction of iLOV and its chromophore completely, given the discrepancy between prediction and the experimental validation for the two mutants characterized here.
We speculate that the discrepancy of the experimental and computational data could arise from higher time scale structural rearrangements of iLOV mutant structures which would require longer simulation trajectories to capture. With the increase and accessibility of higher computing powered systems, it is reasonable to expect that the gap between simulations and experiments would be closed in the near future. Having an iterative approach by coupling computational analyses with high throughput directed evolution studies of LOV proteins could result in more efficient optimization processes of the LOV protein family.

In this study, we could identify the single mutant iLOV^{V392K}, to our knowledge the FbFP displaying the most red-shifted emission peak (518 nm). This mutant displays similar excitation and emission characteristics as iLOV$^{V392K/F410V/A426S}$, while being 10-times brighter. However, iLOV^{V392K} is still 10-times less bright than iLOV. Due to the inherent low brightness of FbFPs this leads to problems in visualizing iLOV^{V392K} *in vivo*, as we could not detect a fluorescent signal using a standard epifluorescence microscope.This might be due to a compromised protein folding. Additionally, the mutants are prone to form aggregates, as we can exclude contamination during the protein purification. A potential contaminant would affect the purified iLOV as well. It remains unknown whether these aggregates are also formed *in vivo*. However, a common structural disruption of tested iLOV mutants seems unlikely, as the two mutants iLOV$^{L470T/Q489K}$ and iLOV^{V392K} do not share common mutations.

A determinant for gene expression, particularly for exogenous gene expression, is the codon usage, due to the codon-usage bias of individual organisms[24]. Initially, we tested an *E. coli* codon-optimized iLOV, which could not be visualized (data not shown). However the mammalian codon-

optimized iLOV could only be detected if an excessive amount of DNA was transfected, which would argue for either limited expression, or a weak brightness of the given fluorescent protein. Due to the lack of a commercial antibody, we can neither confirm the expression of a specific iLOV mutant, nor its tendency to form aggregates *in vivo*.

Previous efforts to improve the usability of iLOV resulted in the generation of phiLOV, an iLOV derivative which possesses a superior photostability, thus tackling one of the major drawbacks in using iLOV[23]. Very recently improved brightness of iLOV variants have been reported[13,14]. It remains to be seen whether the introduced mutations responsible for the increased photostability and brightness of new iLOV variants can be applied to improve the visualization of $iLOV^{V392K}$, without interfering with its excitation and emission spectra.

Declaration of Conflict of Interest

The authors have no conflict of interest to declare.

Acknowledgments

We thank Alexander Löwer (Max Dellbrück Center for molecular Medicine, Berlin) for sharing the H1299 cell line, and Michael Davidson for sharing his iLOV-N1 vector with us.

Figures and Legends

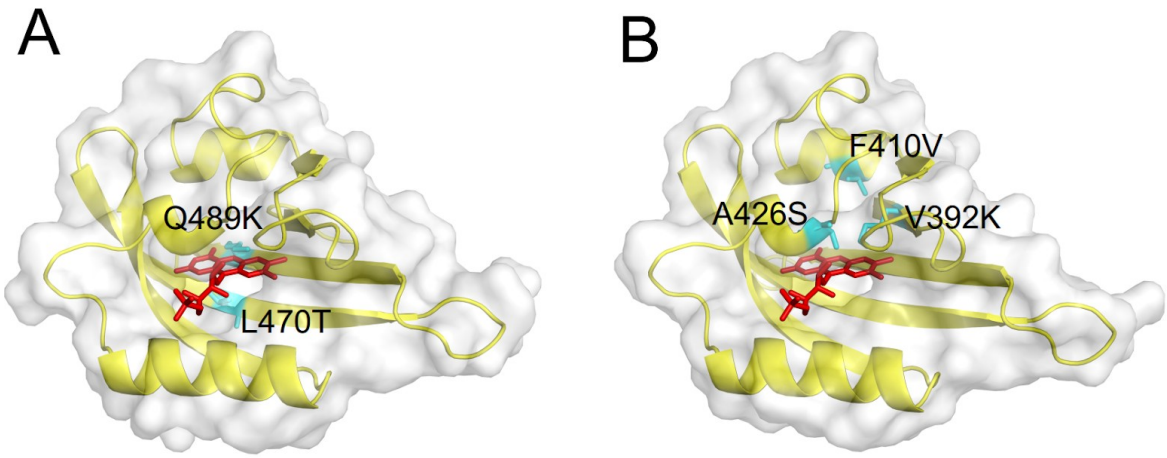

Figure 1: Model structures of iLOV$^{L470T/Q489K}$ and iLOV$^{V392K/F410V/A426S}$ mutants. Cartoon and surface representation of iLOV structures with applied mutations (cyan). Mutant iLOV model structures (yellow) were generated by Swiss-Model web-server[25] and FMN structures (red) were placed by aligning model outputs to WT iLOV X-ray structure (PDB id: 4EEP). Figures were generated by PyMOL[26].

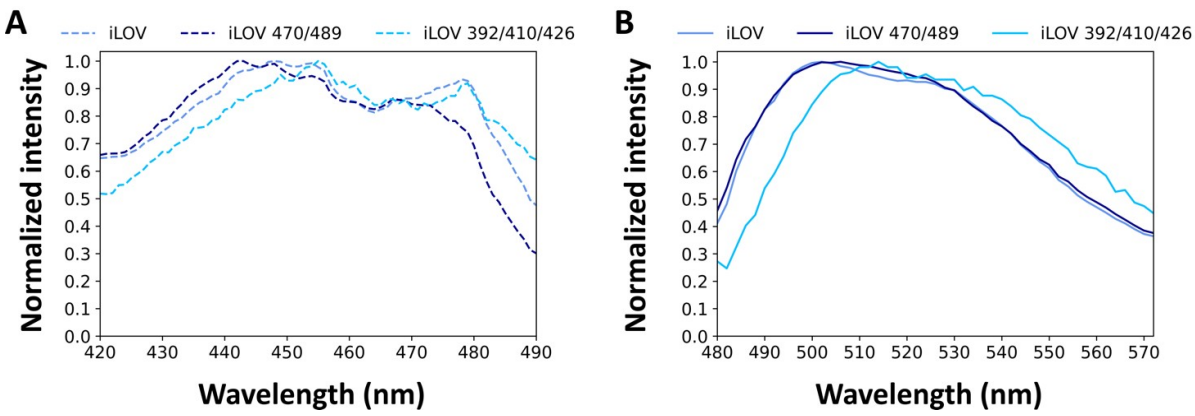

Figure 2: Excitation and emission spectra of purified iLOV variants.

Excitation (A) and emission (B) spectra of the indicated iLOV variants (c = 50µl). Values of the respective spectra were corrected by subtracting the blank (storage buffer), and then normalized to the highest value of the respective spectra to simplify visualization and comparison.

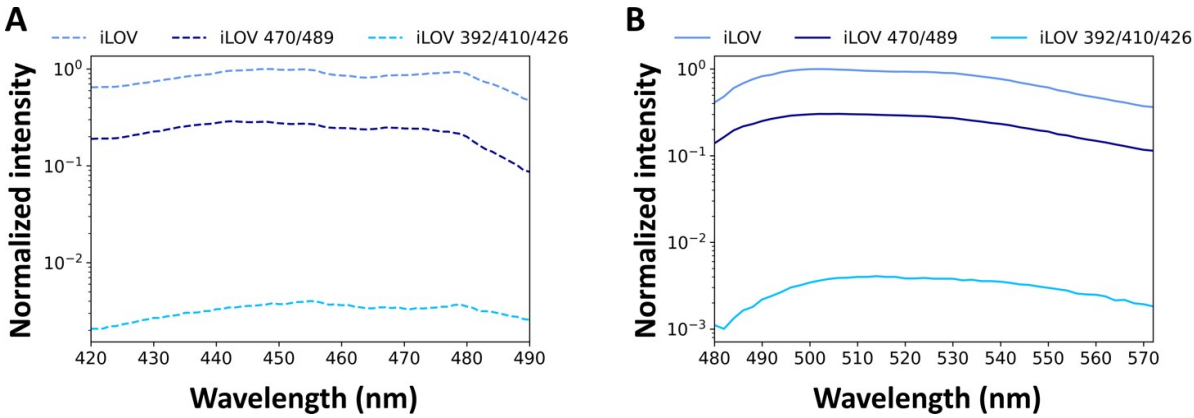

Figure 3: Introduced mutations lead to a reduction in fluorescent intensity.

Excitation (A) and emission (B) spectra of the indicated iLOV variants (c = 50µl). Values of the respective spectra were corrected by subtracting the blank (storage buffer), and then normalized to the highest value of all three spectra, here iLOV.

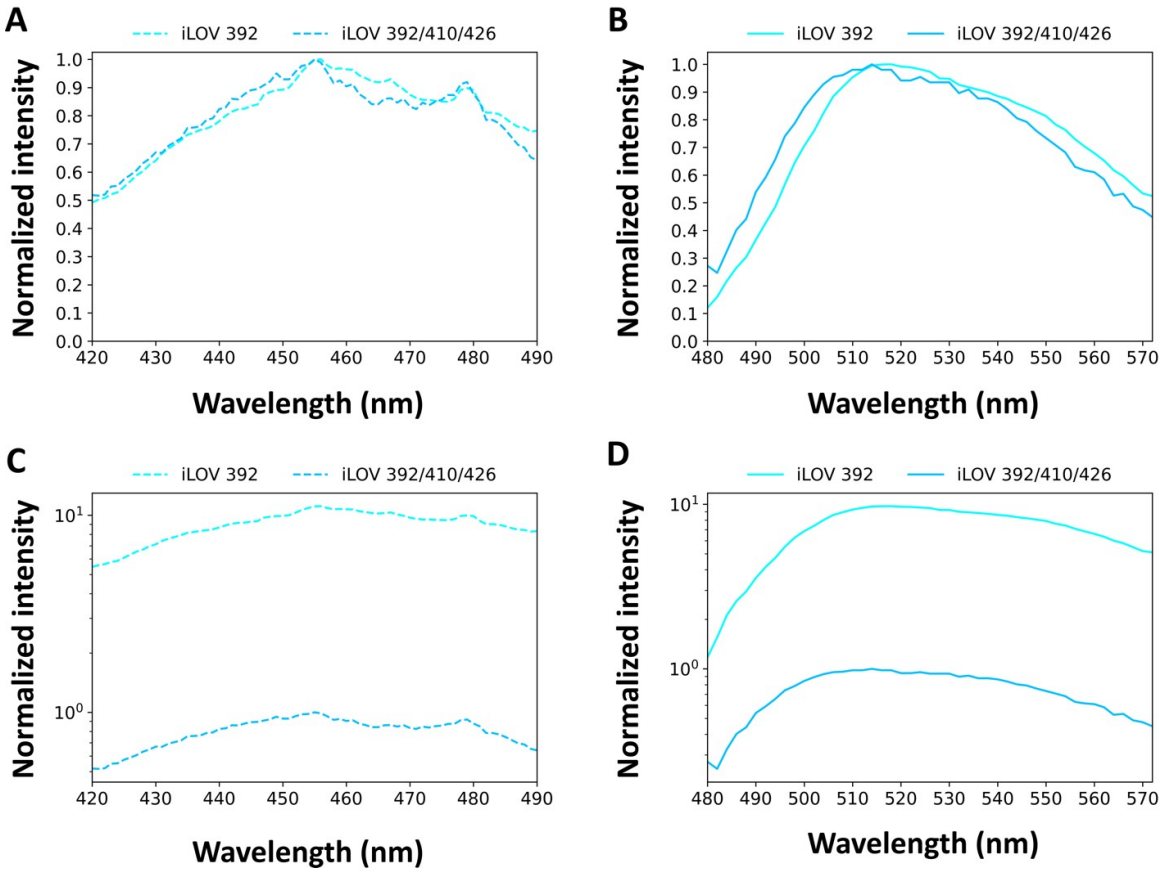

Figure 4: Comparison of the excitation - emission spectra of iLOV^{V392K} and iLOV$^{V392K/F410V/A426S}$ mutants

Excitation (A, C) and emission (B, D) spectra of the indicated iLOV variants (c = 50µl). Values of the respective spectra were corrected by subtracting the blank (storage buffer), and then normalized to the highest value of the respective spectrum (A, B) or to the highest value of the respective spectrum of iLOV$^{V392K/F410V/A426S}$ (C, D).

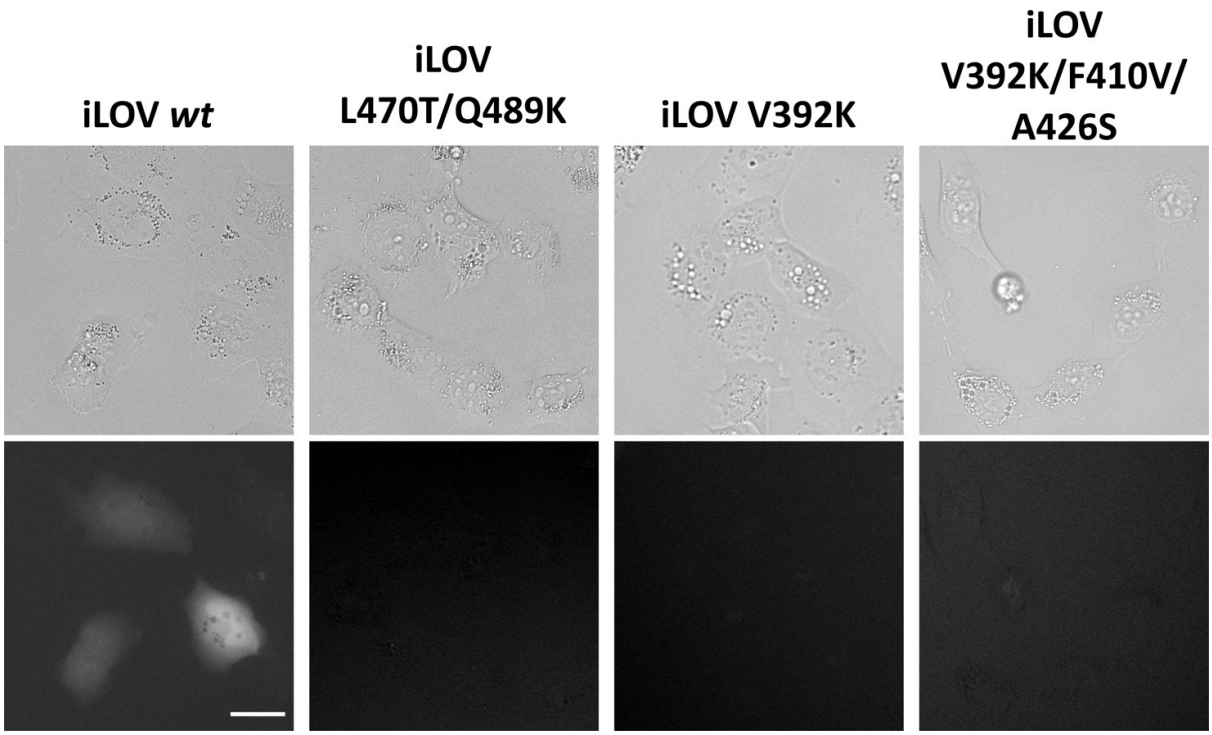

Figure 5: Analysis of iLOV variants in fluorescence microscopy.

Representative bright field (top) and eGFP (bottom) images of H1299 cells transiently transfected with the indicated iLOV construct. Scale bar, 30µm.

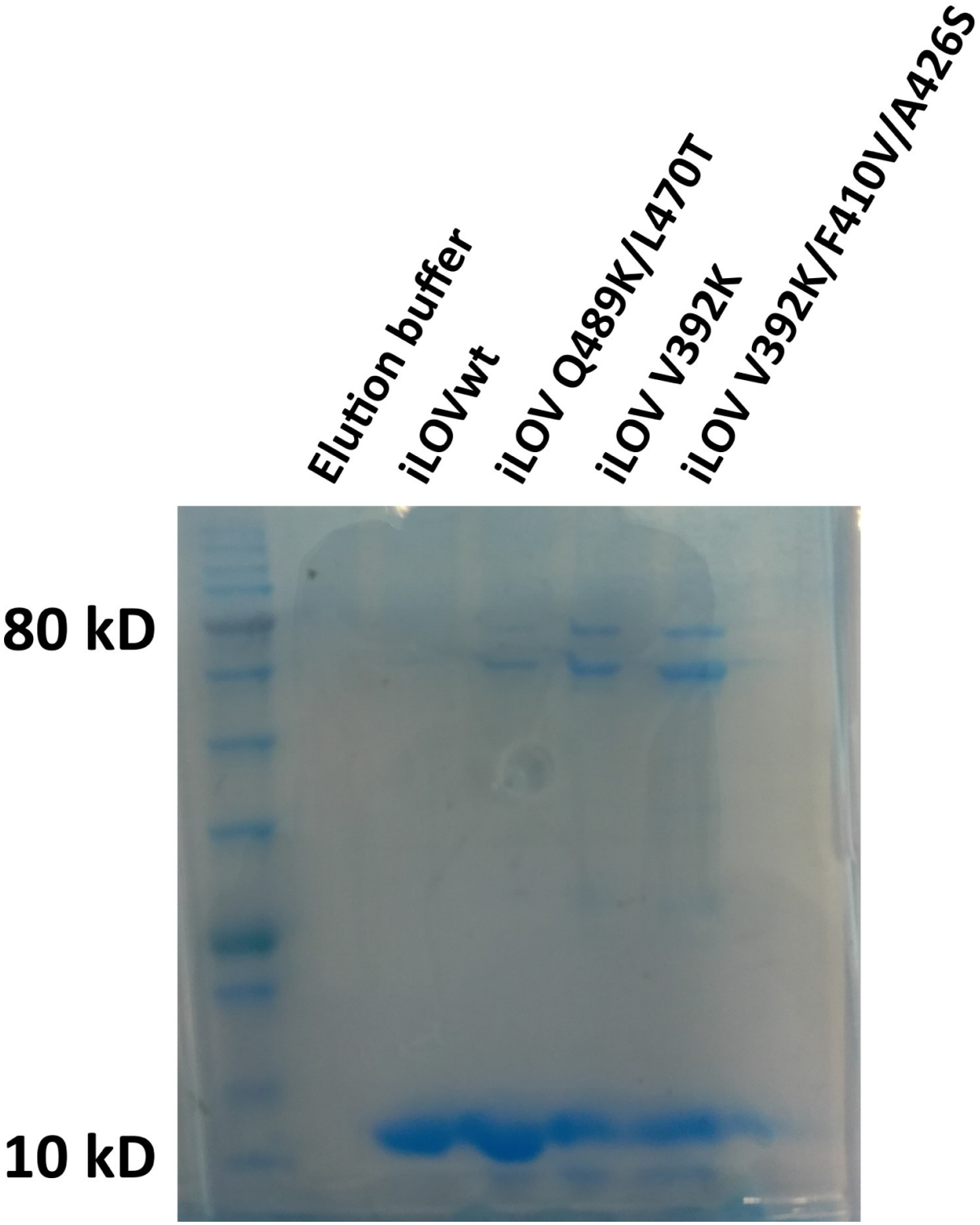

Supplementary Figure 1: SDS gel of purified proteins.

1 µg of the indicated purified protein was diluted in 10 µl storage buffer, boiled and run on a SDS gel.

Table Legends

Table I: Summary of the excitation and emission peaks of characterized iLOV variants.

Overview of all excitation and emission peaks measured in this study and previously predicted by Khrenova et al. [19].

iLOV	WT	L470T/Q489K	V392K/F410V/A426S	V392K
λmax excitation (nm)	448	443 (predicted [19]: 475)	455 (predicted [19]: 498)	456
λmax emission (nm)	500	506 (predicted [19]: 539)	514 (predicted [19] 535)	518

Supplementary Table I: List of Plasmids used in this study.

Primer id	Construct Name	Insert	Backbone	Source
PL01	pcDNA3.1_iLOV	iLOV	pcDNA3.1(+)	this study
PL02	pcDNA3.1_iLOV Q489K	iLOV Q489K	pcDNA3.1(+)	this study
PL03	pcDNA3.1_iLOV L470T-Q489K	iLOV L470T-Q489K	pcDNA3.1(+)	this study
PL04	pcDNA3.1_iLOV V392K	iLOV V392K	pcDNA3.1(+)	this study
PL05	pcDNA3.1_iLOV V392K-A426S	iLOV V392K-A426S	pcDNA3.1(+)	this study
PL06	pcDNA3.1_iLOV V392K-F410V-A426S	iLOV V392K-F410V-A426S	pcDNA3.1(+)	this study
PL07	pET28A_iLOV	iLOV	pET28a	this study

PL08	pET28A_iLOV L470T-Q489K	iLOV L470T-Q489K	pET28a	this study
PL09	pET28A_iLOV V392K	iLOV V392K	pET28a	this study
PL10	pET28A_iLOV V392K-F410V-A426S	iLOV V392K-F410V-A426S	pET28a	this study

Supplementary Table II: List of Oligonucleotides used in this study.

Primer id	Primer	Sequence	Backbone
OL01	iLOVwt_fw_Hind3	TTTT aagctt ATGATCGAGAAGAACTTCGT	pcDNA3.1(+)
OL02	iLOVwt_rv_EcoRI	TTTT gaattc TCACACGTGGTCGCTGCCGT	pcDNA3.1(+)
OL03	iLOV_Q489K_rv_EcoRI	TTTT gaattc TCACACGTGGTCGCTGCCGT CCAGtttCACGCCGATGAAGT ACTGCA	pcDNA3.1(+)
OL04	iLOV_V392K_Hind_fw	TTTT aagctt ATGATCGAGAAGAACTTCaaa ATCACCGACCCCAGA	pcDNA3.1(+)
OL05	iLOV_A426S_fw_Xba1	TTTT tctAGA TTCCTGCAGGGCCCCG	pcDNA3.1(+)
OL06	iLOV_A426S_rv_Xba1	tttt TCTaga GTTTCTGCCCAGGATCT	pcDNA3.1(+)
OL07	iLOV_F410V_fw_BbS	TTTT GAAGAC TT gtgC tggagctgaccgagtacagcagaga	pcDNA3.1(+)

OL08	iLOV_F410V_rv_BbS	TTTT GAAGAC TT Gcac gccgtcgctggcgaagatgatgggg	pcDNA3.1(+)
OL09	iLOV_L470T_fw_BbS	TTTT GAAGAC TT Gacc cacctgcagcccgtgagagaccaga	pcDNA3.1(+)
OL10	iLOV_L470T_rv_BbS	TTTT GAAGAC TT ggtC aggttccagaacttcttgccgctct	pcDNA3.1(+)
OL11	pET28_iLOV_Nde1_fw	TTTT CATATG atcgagaagaacttcgtga	pET28a
OL12	pET28_iLOV_V392K_Nde1_fw	TTTT CATATG atgatcgagaagaacttc	pET28a
OL13	pET28_iLOV_Xho1_rv	TTTT CTCGAG tcacacgtggtcgctgccg	pET28a

References:

(1) Shaner, N. C.; Patterson, G. H.; Davidson, M. W. Advances in Fluorescent Protein Technology. *J. Cell Sci.* **2007**, *120* (Pt 24), 4247–4260. https://doi.org/10.1242/jcs.005801.

(2) Pédelacq, J.-D.; Cabantous, S.; Tran, T.; Terwilliger, T. C.; Waldo, G. S. Engineering and Characterization of a Superfolder Green Fluorescent Protein. *Nat. Biotechnol.* **2006**, *24* (1), 79–88. https://doi.org/10.1038/nbt1172.

(3) Shaner, N. C.; Lambert, G. G.; Chammas, A.; Ni, Y.; Cranfill, P. J.; Baird, M. A.; Sell, B. R.; Allen, J. R.; Day, R. N.; Israelsson, M.; Davidson, M. W.; Wang, J. A Bright Monomeric Green Fluorescent Protein Derived from Branchiostoma Lanceolatum. *Nat. Methods* **2013**, *10* (5), 407–409. https://doi.org/10.1038/nmeth.2413.

(4) Tsien, R. Y. The Green Fluorescent Protein. *Annu. Rev. Biochem.* **1998**, *67* (1), 509–544. https://doi.org/10.1146/annurev.biochem.67.1.509.

(5) Coralli, C.; Cemazar, M.; Kanthou, C.; Tozer, G. M.; Dachs, G. U. Limitations of the Reporter Green Fluorescent Protein under Simulated Tumor Conditions. *Cancer Res.* **2001**, *61* (12), 4784–4790.

(6) Reid, B. G.; Flynn, G. C. Chromophore Formation in Green Fluorescent Protein. *Biochemistry* **1997**, *36* (22), 6786–6791. https://doi.org/10.1021/bi970281w.

(7) Chapman, S.; Faulkner, C.; Kaiserli, E.; Garcia-Mata, C.; Savenkov, E. I.; Roberts, A. G.;

Oparka, K. J.; Christie, J. M. The Photoreversible Fluorescent Protein ILOV Outperforms GFP as a Reporter of Plant Virus Infection. *Proc. Natl. Acad. Sci. U. S. A.* **2008**, *105* (50), 20038–20043. https://doi.org/10.1073/pnas.0807551105.

(8) Roberts, T. M.; Rudolf, F.; Meyer, A.; Pellaux, R.; Whitehead, E.; Panke, S.; Held, M. Identification and Characterisation of a PH-Stable GFP. *Sci. Rep.* **2016**, *6* (1), 28166. https://doi.org/10.1038/srep28166.

(9) Advanced in vivo applications of blue light photoreceptors as alternative fluorescent proteins - Photochemical & Photobiological Sciences (RSC Publishing) https://pubs.rsc.org/en/content/articlelanding/2013/pp/c3pp50040c#!divAbstract (accessed Nov 11, 2020).

(10) Characterization of flavin-based fluorescent proteins: an emerging class of fluorescent reporters - PubMed https://pubmed.ncbi.nlm.nih.gov/23741385/ (accessed Nov 11, 2020).

(11) Mukherjee, A.; Schroeder, C. M. Flavin-Based Fluorescent Proteins: Emerging Paradigms in Biological Imaging. *Curr. Opin. Biotechnol.* **2015**, *31*, 16–23. https://doi.org/10.1016/j.copbio.2014.07.010.

(12) Chia, H. E.; Marsh, E. N. G.; Biteen, J. S. Extending Fluorescence Microscopy into Anaerobic Environments. *Curr. Opin. Chem. Biol.* **2019**, *51*, 98–104. https://doi.org/10.1016/j.cbpa.2019.05.008.

(13) Ko, S.; Hwang, B.; Na, J.-H.; Lee, J.; Jung, S. T. Engineered Arabidopsis Blue Light Receptor LOV Domain Variants with Improved Quantum Yield, Brightness, and Thermostability. *J. Agric. Food Chem.* **2019**, *67* (43), 12037–12043. https://doi.org/10.1021/acs.jafc.9b05473.

(14) Ko, S.; Jeon, H.; Yoon, S.; Kyung, M.; Yun, H.; Na, J.-H.; Jung, S. T. Discovery of Novel Pseudomonas Putida Flavin-Binding Fluorescent Protein Variants with Significantly Improved Quantum Yield. *J. Agric. Food Chem.* **2020**, *68* (21), 5873–5879. https://doi.org/10.1021/acs.jafc.0c00121.

(15) Battad, J. M.; Wilmann, P. G.; Olsen, S.; Byres, E.; Smith, S. C.; Dove, S. G.; Turcic, K. N.; Devenish, R. J.; Rossjohn, J.; Prescott, M. A Structural Basis for the PH-Dependent Increase in Fluorescence Efficiency of Chromoproteins. *J. Mol. Biol.* **2007**, *368* (4), 998–1010. https://doi.org/10.1016/j.jmb.2007.02.007.

(16) Henderson, J. N.; Osborn, M. F.; Koon, N.; Gepshtein, R.; Huppert, D.; Remington, S. J. Excited State Proton Transfer in the Red Fluorescent Protein MKeima. *J. Am. Chem. Soc.* **2009**, *131* (37), 13212–13213. https://doi.org/10.1021/ja904665x.

(17) Khrenova, M. G.; Nemukhin, A. V.; Domratcheva, T. Theoretical Characterization of the

Flavin-Based Fluorescent Protein ILOV and Its Q489K Mutant. *J. Phys. Chem. B* **2015**, *119* (16), 5176–5183. https://doi.org/10.1021/acs.jpcb.5b01299.

(18) Davari, M. D.; Kopka, B.; Wingen, M.; Bocola, M.; Drepper, T.; Jaeger, K.-E.; Schwaneberg, U.; Krauss, U. Photophysics of the LOV-Based Fluorescent Protein Variant ILOV-Q489K Determined by Simulation and Experiment. *J. Phys. Chem. B* **2016**, *120* (13), 3344–3352. https://doi.org/10.1021/acs.jpcb.6b01512.

(19) Khrenova, M. G.; Meteleshko, Y. I.; Nemukhin, A. V. Mutants of the Flavoprotein ILOV as Prospective Red-Shifted Fluorescent Markers. *J. Phys. Chem. B* **2017**, *121* (43), 10018–10025. https://doi.org/10.1021/acs.jpcb.7b07533.

(20) Oliphant, T. E. Python for Scientific Computing. *Comput. Sci. Eng.* **2007**, *9* (3), 10–20. https://doi.org/10.1109/MCSE.2007.58.

(21) McKinney, W. Data Structures for Statistical Computing in Python; Austin, Texas, 2010; pp 56–61. https://doi.org/10.25080/Majora-92bf1922-00a.

(22) Hunter, J. D. Matplotlib: A 2D Graphics Environment. *Comput. Sci. Eng.* **2007**, *9* (3), 90–95. https://doi.org/10.1109/MCSE.2007.55.

(23) Christie, J. M.; Hitomi, K.; Arvai, A. S.; Hartfield, K. A.; Mettlen, M.; Pratt, A. J.; Tainer, J. A.; Getzoff, E. D. Structural Tuning of the Fluorescent Protein ILOV for Improved Photostability. *J. Biol. Chem.* **2012**, *287* (26), 22295–22304. https://doi.org/10.1074/jbc.M111.318881.

(24) Plotkin, J. B.; Kudla, G. Synonymous but Not the Same: The Causes and Consequences of Codon Bias. *Nat. Rev. Genet.* **2011**, *12* (1), 32–42. https://doi.org/10.1038/nrg2899.

(25) Biasini, M.; Bienert, S.; Waterhouse, A.; Arnold, K.; Studer, G.; Schmidt, T.; Kiefer, F.; Cassarino, T. G.; Bertoni, M.; Bordoli, L.; Schwede, T. SWISS-MODEL: Modelling Protein Tertiary and Quaternary Structure Using Evolutionary Information. *Nucleic Acids Res.* **2014**, *42* (W1), W252—-W258. https://doi.org/10.1093/nar/gku340.

(26) The PyMOL Molecular Graphics System, Version 1.7.2.1 Schrödinger, L. *PyMOL*.